HHS Public Access

Author manuscript

Proc SPIE Int Soc Opt Eng. Author manuscript; available in PMC 2018 October 23.

Published in final edited form as:

Proc SPIE Int Soc Opt Eng. 2017 February ; 10140: . doi:10.1117/12.2250428.

Integrative Analysis on Histopathological Image for Identifying Cellular Heterogeneity

Young Hwan Chang, **Guillaume Thibault**, **Brett Johnson**, **Adam Margolin**, and **Joe W. Gray**

Biomedical Engineering, Oregon Health and Science University, Portland, OR, USA

Abstract

This study has brought together image processing, clustering and spatial pattern analysis to quantitatively analyze hematoxylin and eosin-stained (H&E) tissue sections. A mixture of tumor and normal cells (intratumoral heterogeneity) as well as complex tissue architectures of most samples complicate the interpretation of their cytological profiles. To address these challenges, we develop a simple but effective methodology for quantitative analysis for H&E section. We adopt comparative analyses of spatial point patterns to characterize spatial distribution of different nuclei types and complement cellular characteristics analysis. We demonstrate that tumor and normal cell regions exhibit significant differences of lymphocytes spatial distribution or lymphocyte infiltration pattern.

Keywords

Spatial pattern analysis; Heterogeneity; H&E stained image

1. INTRODUCTION

Recent studies show the importance of quantifying not only the abundance and types of cells, but also their spatial locations; for example, the amount of co-localized cancer and immune hotspots weighted by tumor area correlates with a better prognosis in estrogen receptor negative breast cancer in univariate and multivariate analysis.[1] Also, many studies show that spatial information on the tumor immune microenvironment is associated with clinical outcome.[2–5] Despite these advances, there has been less attention on integrative analysis of histology sections. In general, many studies on H&E section can be divided into mainly two different directions:[6,7] 1) local / structural segmentation, 2) large-scale (patch-level) analysis.

The first group of researchers focuses on local structural segmentation, for instance, tumor grading through nuclei segmentation followed by cellular classification. The problem of cell segmentation has received increasing attention in past years and several automated segmentation methods have been proposed.[8] Most methods use a combination of basic algorithms for segmentation, such as intensity thresholding, filtering, morphological

Further author information: (Send correspondence to Young Hwan Chang.) Young Hwan Chang: chanyo (at) ohsu [dot] edu, Telephone: +1 (510) 684-4755.

operations, region accumulation or deformable models.[7] However, since the majority of these approaches treat microscope images as general natural images and methods proposed in recent times are often merely new combination of the existing approaches, the performance and applicability of the proposed methods still remain limited for full automation and large scale analysis, i.e., whole H&E slide section analysis. Moreover, cellular heterogeneity has remain a significant bottleneck in automated image analysis.

The second group of researchers advocates patch-level analysis for tumor representation and classification of histology sections by engineering features and designing classifiers. Image patch classification is an important task in many different medical imaging applications.[9,10] For example, many researchers propose to use image features to discriminate epithelium and stroma, or to perform image patch classification in order to differentiate various tissue patterns. In these studies, various classifiers (Bayesian, *k*-nearest neighbors, support vector machine, etc.) are investigated in a supervised fashion with labeled data by a pathologist visually examining individual cells, which is time-consuming and often infeasible for large-scale studies.

To address these challenge and further understand spatial information, we adopt methods from other disciplines, and propose an integrative analysis of histology section. We demonstrate the concept of extracting and quantifying information contained in imaging data, and show that spatial pattern analysis could complement cellular characteristics analysis by distinguishing different spatial arrangements, such as pattern of lymphocyte infiltration along with different nuclei types or regions.

2. OVERVIEW: NUCLEI SEGMENTATION AND CLUSTERING

In general, many state-of-art segmentation algorithms that perform well on natural image benchmarks tend to perform poorly when applied to biomedical images. This is because the image cues they rely on tend not to be discriminative enough to segment structures such as cell nuclei, stromal cells and tissue fragments. For example, since different classes of nuclei show various textural and morphological characteristics and exhibit irregular shapes, it is a challenging task to develop automated nuclei segmentation algorithm, which is flexible enough to cope with biological heterogeneities (e.g., different nuclei types) and technical variations (e.g., staining, fixation).

Here, we use our automatic nuclei segmentation algorithm.[11] In H&E stained section, since hematoxylin stains cell nuclei blue while eosin stains other structures in various shades from red to pink,[12] and each pixel represents a part of morphological features, by mapping each pixel with useful morphological features and grouping neighboring pixels with similar features, one can differentiate between foreground and background, or between different tissues and cells or nuclei. Thus, nuclei segmentation can be effectively performed by partitioned groups. Also, we can exclude smaller region and artifacts to avoid unusual prediction based on their morphological features. More detailed information can be found in our previous work.[11]

Once we segment individual nuclei in the H&E section, we can obtain morphological characteristics of individual nuclei by measuring various features including area, major/minor axis length, perimeter, equivalent diameter, shape indices and intensity.[13] Then, one can use these features for clustering individual nuclei into different types, because measured features describe the characteristics of individual nuclei. For example, lymphocytes shown in Figure 2 (left) have a typical morphology of small, round and homogeneously basophilic nuclei, thus can be reliably differentiated from other cell types. To do this, we adopt a Landmark-based Spectral Clustering (LSC)[14] for large scale clustering because the whole H&E slide sections consist of tens of thousand or hundreds of thousand nuclei. LSC selects a few representative data points as the landmarks so one can treat the basis vectors as the landmark points from a data set. Thus, we can cluster individual segmented nuclei into different types based on the landmark-based representation.

3. COMPARATIVE ANALYSES OF SPATIAL POINT PATTERNS

In general, spatial arrangement and architectural organization of nuclei is generally not reflected in cellular profiles, and thus this rich information is underused. Also, biological heterogeneities (e.g., various nuclei types) and high redundancy in the feature representations can degrade the performance of classifier.[15] To address this issue, we adopted spatial pattern analysis to characterize spatial distribution across different nuclei types and complement cellular characteristics analysis in our previous work.[11] For example, for given points of the same nuclei type, our interest lies in the detection of spatial patterns in their distribution. In addition, if there are more than one set of points, spatial patterns may be found in the relationship between point distributions.[16,17] In this section, first we briefly summarize our previous work,[11] which is necessary for describing our current work and describe the extended work.

3.1 Previous work: Spatial Point Pattern Analysis

Consider the following point patterns as shown in Figure 1 (a–c) and ask the interesting question “how one statistically can distinguish these patterns without knowing anything else about them”. In general, one can develop a benchmark model for spatial point patterns that is called *complete spatial randomness* (CSR), and test each of these patterns against CSR pattern[16] as shown in Figure 1(d) and (e). Note that under CSR, events are distributed independently and uniformly over the study region R (i.e., no influence on one another).

There are mainly three approaches to test the CSR hypothesis: the *quadrat* method, the *nearest-neighbor method*, and the method of *K-functions*. Here, in order to consider scale effects and capture a range of scales in a systematic way, we consider randomly sampled point event of varying sizes of d. The K-function is defined as $\hat{K}(d) = \frac{1}{\lambda}E$ [# of additional events within distance d of an arbitrary event], where λ is the density (number per unit area) of events. As with a certain distances, $\hat{K}(d)$ yields information about clustering and dispersion. For a CSR spatial point process, the theoretical K-function is $K(d) = \pi d^2$. Thus, when $\hat{K}(d) > \pi d^2$, this indicates some degree of clustering at scale d (i.e., a mean point count is higher than would be expected under CSR) as shown in Figure 1(d). On the other hand, a value $\hat{K}(d) > \pi d^2$ indicates some degree of dispersion at scale d. Based on the K-

function, another approach is to transform $\hat{K}(d)$ using $\hat{L}(d) = \sqrt{\frac{\hat{K}(d)}{\pi}} - d$. Peaks of positive values in a plot of $\hat{L}(d)$ would correspond to clustering and negative values indicating regularity, for the corresponding scale d as shown in Figure 1(e). It should be noted that K-function is defined for a stationary, spatially homogeneous point process only, i.e., the average density within point pattern is assumed to be independent of the spatial location. In our previous work,[11] we focused on analyzing single point pattern against CSR using K-function analysis. We characterized a spatial distribution of dominant nuclei type along the different regions and observe that tumor nuclei are differentially distributed as shown in Figure 2 (right) where we select three representative regions (tumor cell, normal cell and lymphocyte region) from the whole slide section shown in Figure 2 (left). Note that we assume a stationary and spatially homogeneous point process within each region.

3.2 Analysis of Spatial Similarity

The relevant and more interesting question involves relationships between more than one pattern. When one compare two populations, the interesting question is usually whether or not these events influence one another in some way or simply, how similar these spatial point patterns are. Hence, analyzing this competition between other cell types or architectural organization resulting from this competition may be interesting. For example, in H&E sections where tumor cells are found, there will invariably be other cells such as lymphocytes competing with tumor cells. Then, we might simply ask whether the pattern of tumor-like cells, S_1, is more clustered than the pattern of lymphocytes, S_2 in the study region **R**.

To do so, we may simply compare marginal distribution of two patterns by examining how the spatial point patterns S_1 and S_2 are similar,[17] instead of analyzing their joint distribution (i.e., cross K-functions to test whether there was significant “attraction” or “repulsion” between two patterns). If the sizes of S_1 and S_2 are given respectively by n_1 and n_2, then null hypothesis is simply that the combination of these two patterns is in fact a single population realization of size n (= n_1 + n_2). If this was true, the sample K-functions, $\hat{K}_1(d)$ and $\hat{K}_2(d)$ should be estimating the same K-function. In this context, “complete similarity” would reduce the simple null hypothesis, $H_0 : K_1(d) = K_2(d)$. However, this simplification is only appropriate for stationary isotropic processes with Ripley correction so we need to characterize “complete similarity” in a way that will allow deviations from this hypothesis to be tested statistically.[17] Even in the absence of stationarity, the sample K-functions continue to be reasonable measures of clustering (or dispersion) within populations. Hence, to test for relative clustering (or dispersion), it is natural to focus on the difference between these sample measure, i.e., $\Delta(d) = \hat{K}_1(d) - \hat{K}_2(d)$. Note that if both samples are indeed coming from the same population, then $\hat{K}_1(d)$ and $\hat{K}_2(d)$ should be estimating the same K-function (*complete similarity*). The relevant spatial similarity hypothesis for this analysis is that the observed difference is not statistically distinguishable from the random differences obtained from realizations of the conditional distribution of labels under the spatial indistinguishability hypothesis*.[17]

Then, if we simulate random relabelings to obtain a sampling distribution of $\Delta(d)$ under this spatial similarity hypothesis, the observed difference can simply be compared with this distribution. Also, one can calculate p-values for various simulations and interpret the p-value output. For instance, if the observed difference is unusually large (small) relative to this distribution, then it can reasonably be inferred that S_1 is significantly more clustered (dispersed) than S_2; This procedure can be summarized by the following simple variation of the random relabeling test:[17]

- Step 1: given $(s_1, \ldots, s_n)$ and $(m_1, \ldots, m_n)$, simulate N random permutations and construct the corresponding the label permutations $(m_{\pi 1(k)}, \ldots, m_{\pi n(k)})$, $k = 1, \ldots, N$.
- Step 2: given S_1^k and S_2^k obtained from $[(s_1, \ldots, s_n), (m_{\pi 1(k)}, \ldots, m_{\pi n(k)})]$, calculate the sample difference values $\Delta^k(d) = \hat{K}_1^k(d) - \hat{K}_2^k(d)$ for each $k = 1, \ldots, N$ and set of relevant radial distances d. If S_1^k and S_2^k denote the population patterns obtained from the joint realization $[(s_1, \ldots, s_n), (m_{\pi 1(k)}, \ldots, m_{\pi n(k)})]$, for the given set of relevant radial distances, $D = \{d_w : w = 1, \ldots, W\}$, calculate the sample difference values $\{\Delta^k(d_w) : w = 1, \ldots, W\}$ for each $k = 1, \ldots, N$ where $\Delta^k(d) = \hat{K}_1^k(d) - \hat{K}_2^k(d)$.
- Step 3: under the spatial similarity hypothesis, from the list of $\Delta^k(d)$ obtained from Step 2, the probability of obtaining a value as large as $\Delta^0(d)$ is estimated by the relative *clustering* p-value for S_1 versus S_2, $\hat{p}^{12}_{dispersed}(d) = \frac{m^0_+ + 1}{N+1}$ where m^0_+ denotes the number of simulated random relabelings with $\Delta^k(d) \geq \Delta^0(d)$. Similarly, the probability of obtaining a value as small as $\Delta^0(d)$ is estimated by the relative *dispersion* p-value for S_1 versus S_2, $\hat{p}^{12}_{dispersed}(d) = \frac{m^0_- + 1}{N+1}$ where m^0_- denotes the number of simulated random relabeling with $\Delta^k(d) < \Delta^0(d)$.

  Under the spatial similarity hypothesis, each observed value $\Delta^0(d_w)$ should be a "typical" sample from the list of values $[\Delta^k(d_w) : k = 0, 1, \ldots, N]$. Hence if we now let m^0_+ denote the number of simulated random relabelings with $\Delta^k(d_w) \geq \Delta^0(d_w)$, then the probability of obtaining a value as large as $\Delta^0(d_w)$ under this hypothesis is estimated by the relative clustering p-value for population 1 versus population 2: $\hat{p}^{12}_{clustered}(d) = \frac{m^0_+ + 1}{N+1}$. Similarly, if m^0_- denotes the number of simulated random relabeling with $\Delta^k(d_w) \leq \Delta^0(d_w)$, then the probability of obtaining a value as small as $\Delta^0(d_w)$ under this hypothesis is estimated by the

---

*S_1 and S_2 satisfy both spatial independence and exchangeability conditions as follows:
(spatial independence): $\Pr[(m_1, \ldots, m_n) | (s_1, \ldots, s_n)] = \Pr(m_1, \ldots, m_n)$
(exchangeability): $\Pr(m_{\pi_1}, \ldots, m_{\pi n}) = \Pr(m_1, \ldots, m_n)$
where m_i, s_i represents event label and location respectively, π_i represents random permutations and $\Pr[(m_1, \ldots, m_n)|(s_1, \ldots, s_n)]$ denotes the conditional distribution of event labels given their locations and $\Pr(m_1, \ldots, m_n)$ denotes marginal distribution of event labels.

following relative dispersion p-value for population 1 versus population 2:

$$\hat{p}^{12}_{dispersed}(d) = \frac{m^0_- + 1}{N + 1}.$$

4. RESULT AND DISCUSSION

We compare two patterns in the study region, for example, since lymphocytes can be reliably differentiated from other nuclei types, we consider S_2 as lymphocyte and S_1 as other cells in the region. We select 15 different regions as shown in Figure 3 (top, (a)-(h): tumor cell regions, (i)-(o): normal cell regions). In Figure 3 (bottom left), we plot population density of S_1 (either tumor cell or normal cell) versus S_2 (lymphocyte) in each region but there is no distinct difference of population density between tumor and normal cell region. However, if we compare spatial similarity between S_1 and S_2, we can clearly observe distinct spatial pattern for those two regions. Figure 3 (bottom middle, tumor region) shows that S_1 is significantly more clustered than S_2 where values below the red dashed line on the bottom (0.05) denotes the significant clustered pattern at the 95 percent confidence interval. On the other hand, in normal cell region (bottom right), we infer that S_1 is significantly more dispersed than S_2 where values above the red dashed line at the top (0.95) denotes significant dispersion at the 95 percent confidence interval. Therefore, we can characterize distinct spatial distribution of nuclei in two different regions, for example, tumor cell nuclei are indeed more clustered than lymphocytes but normal cell nuclei are strongly dispersed within radius (<100 pixels) than lymphocytes. In other words, spatial distributions of lymphocyte are different between tumor cell region and normal cell region although there is no distinct difference in the population.

5. CONCLUSIONS

In this work, we propose simple but effective methods for an integrative analysis on H&E section. We demonstrate that spatial pattern analysis could complement cellular characteristics analysis. We also characterize spatial distribution of lymphocytes in the study region and find that lymphocyte infiltrations are different between tumor cell region and normal cell region.

ACKNOWLEDGMENTS

This research was supported in part by start-up funds from Oregon Health and Science University.

REFERENCES

[1]. Nawaz S, Heindl A, Koelble K, and Yuan Y, “Beyond immune density: critical role of spatial heterogeneity in estrogen receptor-negative breast cancer,” Mod Pathol 28, 766–777 (06 2015). [PubMed: 25720324]

[2]. L. S, S. N, and P. F, “Prognostic and predictive value of tumor-infiltrating lymphocytes in a phase iii randomized adjuvant breast cancer trial in node-positive breast cancer comparing the addition of docetaxel to doxorubicin with doxorubicin-based chemotherapy: Big 02–98,” J Clin Oncol 31, 860–867 (2013). [PubMed: 23341518]

[3]. I.-N. Y, D.-E. S, and L. S, “Prospective validation of immunological infiltrate for prediction of response to neoadjuvant chemotherapy in her2-negative breast cancer[mdash]a substudy of the neoadjuvant geparquinto trial,” PLoS One 8, e79775– (2013). [PubMed: 24312450]

[4]. Y Y, F H, and OM R, “Quantitative image analysis of cellular heterogeneity in breast tumors complements genomic profiling,” Sci Transl Med 4, – (2012).

[5]. G. J, C. A, and S.-C. F, “Type, density, and location of immune cells within human colorectal tumors predict clinical outcome,” Science 313, 1960–1964 (2006). [PubMed: 17008531]

[6]. Gurcan M, Boucheron L, Can A, Madabhushi A, Rajpoot N, and Yener B, “Histopathological image analysis: A review,” Biomedical Engineering, IEEE Reviews in 2, 147–171 (2009).

[7]. Irshad H, Veillard A, Roux L, and Racoceanu D, “Methods for nuclei detection, segmentation, and classification in digital histopathology: A review - current status and future potential,” Biomedical Engineering, IEEE Reviews in 7, 97–114 (2014).

[8]. Meijering E, “Cell segmentation: 50 years down the road [life sciences],” Signal Processing Magazine, IEEE 29, 140–145 (9 2012).

[9]. Bianconi F, Álvarez Larrán A, and Fernández A, “Discrimination between tumour epithelium and stroma via perception-based features,” Neurocomput. 154, 119–126 (Apr. 2015).

[10]. Li Q, Cai W, and Feng D, “Lung image patch classification with automatic feature learning,” in [con], 6079–6082 (7 2013).

[11]. Chang YH, Thibault G, Azimi V, et al., “Quantitative analysis of histological tissue image based on cytological profiles and spatial statistics,” in [38th Annual International Conference of the IEEE Engineering in Medicine and Biology Society], 248–255, IEEE (2016).

[12]. Wang C-W, “Robust automated tumour segmentation on histological and immunohistochemical tissue images,” PLoS ONE 6(2) (2011).

[13]. Jones TR, Carpenter AE, Lamprecht MR, Moffat J, Silver SJ, Grenier JK, Castoreno AB, Eggert US, Root DE, Golland P, and Sabatini DM, “Scoring diverse cellular morphologies in image-based screens with iterative feedback and machine learning,” Proceedings of the National Academy of Sciences 106(6), 1826–1831 (2009).

[14]. Cai D and Chen X, “Large scale spectral clustering via landmark-based sparse representation,” Cybernetics, IEEE Transactions on 45, 1669–1680 (8 2015).

[15]. Zhou Y, Chang H, Barner K, Spellman P, and Parvin B, “Classification of histology sections via multispectral convolutional sparse coding,” in [Computer Vision and Pattern Recognition (CVPR), 2014 IEEE Conference on], 3081–3088 (6 2014).

[16]. Martinez WL and Martinez AR, [Computational Statistics Handbook with MATLAB, Second Edition], Chapman and Hall/CRC, 2 ed (2007).

[17]. Smith T, “Notebook on spatial data analysis.” Lecture Note (2016).

[18]. Carpenter AE, Jones TR, Lamprecht MR, Clarke C, Kang I, Friman O, Guertin DA, Chang J, Lindquist RA, Moffat J, Golland P, and Sabatini DM, “Cellprofiler: image analysis software for identifying and quantifying cell phenotypes,” Genome Biology 7(10), 1–11 (2006).

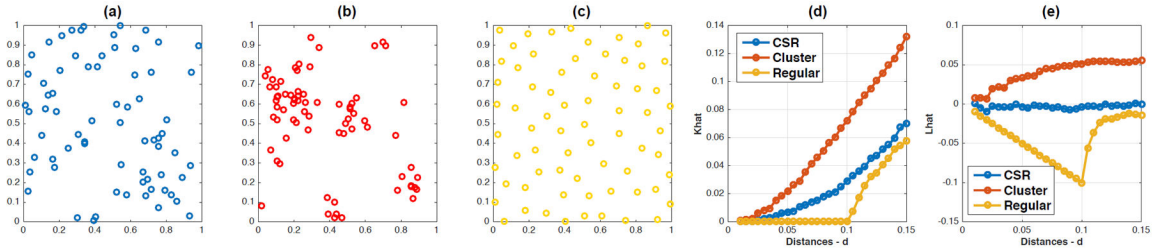

Figure 1.

Examples of spatial point patterns: (a) represents the CSR point process, (b) represents the cluster point pattern, (c) represents point pattern exhibiting regularity, (d) *K*-function analysis and (e) *L*-function analysis.

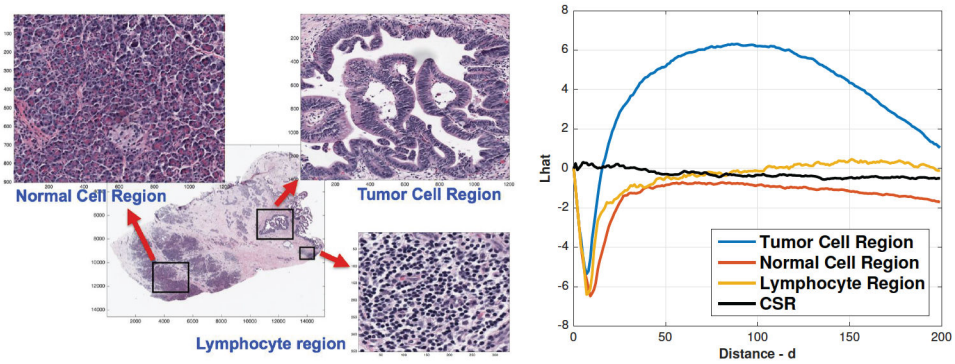

Figure 2.

(left) we select three representative regions such as tumor cell, normal cell and lymphocyte region (right) higher nuclei clustering was found in tumor region compared with normal cell or lymphocyte region based on $\hat{L}$ function, possibly due to the aggregated patterns of tumor cells.[11]

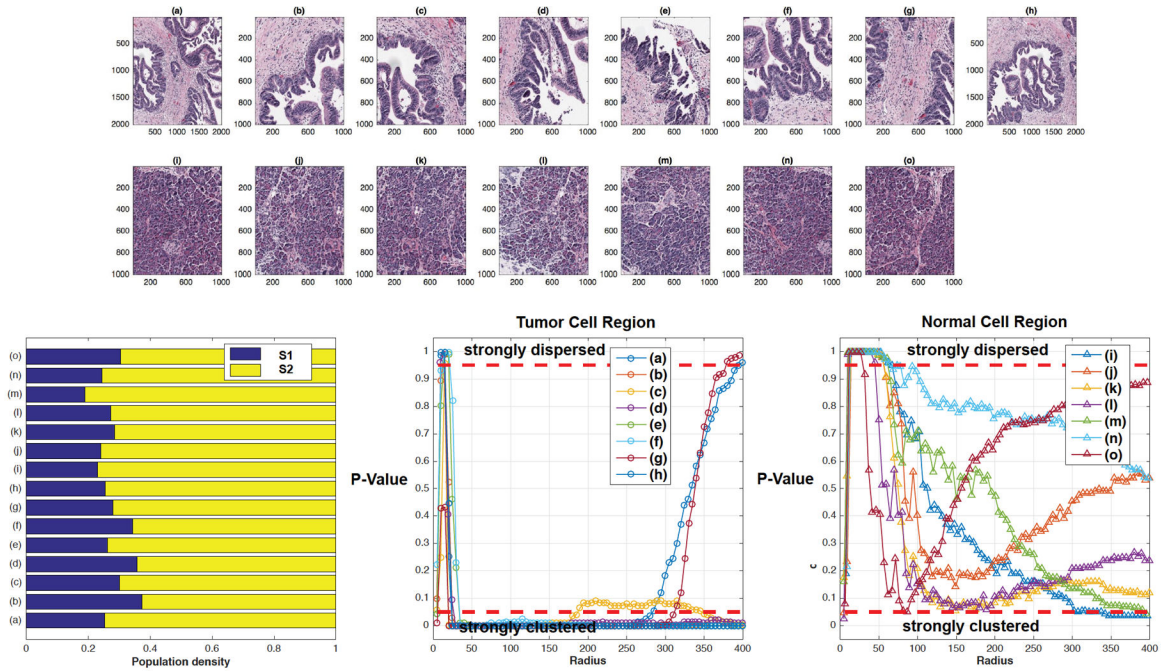

Figure 3.

(top) different regions chosen from the whole slide section (bottom) population density and spatial similarity analysis (S_1 versus S_2) for tumor cell region and normal cell region where values below the red dashed line on the bottom (0.05) denotes the significant clustered pattern at the 95 percent confidence interval and values above the red dashed line at the top (0.95) denotes significant dispersion at the 95 percent confidence interval.